Molecular calculations of excitation energies and (hyper)polarizabilities.

Schipper, P.R.T.; Gritsenko, O.V.; van Gisbergen, S.J.A.; Baerends, E.J.

published in
Journal of Chemical Physics
2000

DOI (link to publisher)
10.1063/1.480688

document version
Publisher's PDF, also known as Version of record

Molecular calculations of excitation energies and (hyper)polarizabilities with a statistical average of orbital model exchange-correlation potentials

P. R. T. Schipper, O. V. Gritsenko, S. J. A. van Gisbergen, and E. J. Baerends[a)]
Scheikundig Laboratorium der Vrije Universiteit, De Boelelaan 1083, 1081 HV Amsterdam, The Netherlands

(Received 23 July 1999; accepted 13 October 1999)

An approximate Kohn–Sham exchange-correlation potential ν_{xc}^{SAOP} is developed with the method of statistical averaging of (model) orbital potentials (SAOP) and is applied to the calculation of excitation energies as well as of static and frequency-dependent multipole polarizabilities and hyperpolarizabilities within time-dependent density functional theory (TDDFT). ν_{xc}^{SAOP} provides high quality results for all calculated response properties and a substantial improvement upon the local density approximation (LDA) and the van Leeuwen–Baerends (LB) potentials for the prototype molecules CO, N_2, CH_2O, and C_2H_4. For the first three molecules and the lower excitations of the C_2H_4 the average error of the vertical excitation energies calculated with ν_{xc}^{SAOP} approaches the benchmark accuracy of 0.1 eV for the electronic spectra. © *2000 American Institute of Physics.* [S0021-9606(00)31102-3]

I. INTRODUCTION

The recent progress of time-dependent density functional perturbation theory (TDDFPT)[1–5] (useful introductions are provided by Refs. 1,2,6) offers an efficient one-electron approach to the calculation of various static and frequency-dependent molecular response properties. At the linear response level excitation energies,[5,7–12] frequency-dependent multipole polarizabilities,[7,13–16] and van der Waals dispersion coefficients[3,14,17] have been calculated. At the nonlinear level, frequency-dependent hyperpolarizabilities were obtained,[18–22] which govern the nonlinear optical (NLO) response properties of molecules.

TDDFPT is rapidly becoming a standard tool for studying these properties. Excitation energies, in particular, can now be obtained from various quantum chemistry packages.[1,4,6,12,16,23,24] The reasons for this rapid growth of interest in molecular applications of TDDFPT are basically the same as those which have made ground state DFT a popular approach to the molecular electronic structure problem. Reasonably accurate results can already be obtained at the simple level of the local density approximation (LDA). These are usually superior in quality to time-dependent Hartree–Fock (TDHF) results for excitation energies and polarizabilities, at a comparable or lower computational cost. The size of the systems for which TDDFPT calculations are still feasible, is roughly the same as those for which a ground state DFT calculation can be performed. Calculations on systems with typically one hundred atoms have already been performed[25–27] and improvements in the algorithms (using, for example, linear scaling techniques) may drastically increase the size of the systems in the near future. TDDFPT also gives reliable results in the case of transition metals compounds[28–30] and double excitations from open shell systems[24] for which TDHF is known to be unreliable. This combination of efficiency and reliability (see, however, Ref. 27 for an exception) explains the growing interest. The main goal of the present paper is to further improve the accuracy which can be obtained from such calculations by improving the approximation to the exchange-correlation potential which is usually the main source of error,[11,31] thus moving closer to the benchmark accuracy obtained in, e.g., coupled-cluster calculations.

The TDDFPT calculations employ the Kohn–Sham (KS) exchange-correlation (XC) potential ν_{xc} as well as the XC kernels f_{xc} and g_{xc}. The potential ν_{xc} represents effects of the electron exchange and the Coulomb correlation in the one-electron KS equations for the stationary ground state,

$$\left\{-\frac{1}{2}\nabla^2+\nu_{ext}(\mathbf{r})+\nu_H(\mathbf{r})+\nu_{xc}(\mathbf{r})\right\}\psi_i(\mathbf{r})=\epsilon_i\psi_i(\mathbf{r}), \qquad (1.1)$$

where ν_{ext} is the external potential and ν_H is the Hartree potential of the electrostatic electron repulsion which, together with the exchange-correlation potential ν_{xc}, define the KS orbitals $\psi_i(\mathbf{r})$, their energies ϵ_i and the electron density $\rho(\mathbf{r})$,

$$\rho(\mathbf{r})=\sum_{i=1}^{N} P_{ii}|\psi_i(\mathbf{r})|^2, \qquad (1.2)$$

where P_{ii} are the occupation numbers (or diagonal elements of the density matrix on a KS orbital basis). The XC kernels f_{xc} and g_{xc} determine in TDDFPT the spatial change and time evolution of ν_{xc} in response to the perturbation $\delta\nu_{ext}(\mathbf{r}t)$ of the external potential,[1]

a)Electronic mail: baerends@chem.vu.nl

$$\nu_{\mathrm{xc}}(\mathbf{r}t)=\nu_{\mathrm{xc}}(\mathbf{r})+\int\int d\mathbf{r}'\,dt'\,f_{\mathrm{xc}}(\mathbf{r}t,\mathbf{r}'t')\,\delta\rho(\mathbf{r}'t') + \frac{1}{2}\int\int\int\int d\mathbf{r}'\,d\mathbf{r}''\,dt'\,dt''\,g_{\mathrm{xc}} \times(\mathbf{r}t,\mathbf{r}'t',d\mathbf{r}''\,dt'')\,\delta\rho(\mathbf{r}'t')\,\delta\rho(\mathbf{r}''t'')+\cdots, \tag{1.3}$$

where $\delta\rho$ is the density response. The relevance of ν_{xc} and f_{xc} for linear response equations in DFT can be explained from the equation from which the first-order density change due to a frequency-dependent electric field is calculated (here we use the frequency domain):

$$\delta\rho(\mathbf{r},\omega)=\int d\mathbf{r}'\,\chi_s(\mathbf{r},\mathbf{r}';\omega)\,\delta\nu_s(\mathbf{r}',\omega). \tag{1.4}$$

The Kohn–Sham (single particle) response function χ_s is calculated from the Kohn–Sham orbitals and orbital energies which are obtained from an ordinary ground-state DFT calculation and which are fully determined by the static xc potential ν_{xc}. The effective KS potential $\delta\nu_s$ contains the external perturbation, as well as Hartree and xc terms which screen this external perturbation. The xc screening is determined by the xc kernel f_{xc}.

The exact ν_{xc}, f_{xc}, and g_{xc} are not known, so that various approximations are in use. In this paper the so-called adiabatic local density approximation (ALDA) is employed for f_{xc} and g_{xc}. These functionals neglect the frequency dependence and the spatial nonlocality of these kernels. The ALDA functionals are computationally very simple and have been used almost without exception in previous molecular TDDFPT calculations. For f_{xc} the ALDA is given by

$$f_{\mathrm{xc}}^{\mathrm{ALDA}}(\mathbf{r},\mathbf{r}',\omega)=\delta(\mathbf{r}-\mathbf{r}')\left.\frac{d\nu_{\mathrm{xc}}^{\mathrm{LDA}}(\mathbf{r})}{d\rho(\mathbf{r}')}\right|_{\rho=\rho_{\mathrm{SCF}}}. \tag{1.5}$$

In other words, it is simply the static derivative of the potential of the LDA. Although one might question the validity of the ALDA on general grounds, several studies have shown[11,31] that (at least for applications to small systems), the largest source of error comes in fact from the approximation to the static xc potential ν_{xc}. This was shown by combining the essentially exact xc potentials generated from *ab initio* densities (which can be done for small systems only) with the ALDA for f_{xc}. In that case, very satisfactory results were obtained,[11] further suggesting the desirability to improve the models for the xc potential. In particular, the traditional local-density approximation (LDA) and generalized gradient approximations (GGAs) for ν_{xc} have met with limited success, which is only partially corrected by functionals which include a fraction of exact exchange. To be specific, although calculations with $\nu_{\mathrm{xc}}^{\mathrm{LDA}}$ of the local density approximation (LDA) produce reasonable lowest excitation energies,[8,32] they significantly and systematically overestimate (hyper)polarizabilities and their frequency dependence and they underestimate higher-lying vertical excitations.[3,4,8,11,33] Standard GGA corrections to $\nu_{\mathrm{xc}}^{\mathrm{LDA}}$ do not produce a substantial improvement of the results.

The van Leeuwen–Baerends (LB)[34] potential $\nu_{\mathrm{xc}}^{\mathrm{LB}}$ with the proper Coulombic asymptotics produces improved (multipole) polarizabilities,[13,14] hyperpolarizabilities,[21] and high-lying excitation energies[8] compared to LDA. Still, the improvement does not hold for all properties; the important lowest excitation energies are usually worse than at the LDA level. (The low-lying excited states in the visible and near-UV region are nevertheless usually the most interesting ones. Photodissociation for instance often proceeds on the lowest excited state surface.) Furthermore, the LB correction to LDA seems to overcorrect in certain cases. Whereas the LDA polarizabilities are usually too large, the LB results are slightly too small on average, while it also tends to predict a too low frequency dependence for $\alpha(\omega)$.[13] This holds to a greater extent for the hyperpolarizabilities for which LDA gives strong overestimations, whereas the LB results are too low.[21] For this case, the LB results do not even improve much upon TDHF results. Recently, specialized asymptotic corrections have been grafted onto the LDA[35] and GGA[5] potentials, which provide the correct Coulombic asymptotics for the potential, $\nu_{\mathrm{xc}}(\mathbf{r})\rightarrow -1/r+C$, $r\rightarrow\infty$, and the rigorous relation for the calculated energy ϵ_N of the highest occupied KS orbital ψ_N in (1.1), $\epsilon_N=\nu_{\mathrm{xc}}(\infty)-I_p$, where I_p is the ionization potential. These corrections have produced considerable improvement of the calculated molecular response properties.

The discussion in this section highlights the importance of accurate modeling of ν_{xc}. In our previous paper[36] a general method of modeling ν_{xc} has been proposed with the statistical average of different model orbital potentials (SAOP) for the occupied KS orbitals $\psi_{i\sigma}$. In this paper an approximate potential $\nu_{\mathrm{xc}}^{\mathrm{SAOP}}$ is developed with the SAOP for the molecular response calculations. In Sec. II the SAOP approach is outlined and functional as well as graphical representations of $\nu_{\mathrm{xc}}^{\mathrm{SAOP}}$ are given. The distinguishing feature of this new potential is that it incorporates physically well motivated features in both the asymptotic region and the (sub)-valence and core regions. In Sec. III the basic formulas of the calculated response properties are presented and the computational scheme is characterized. In Sec. IV $\nu_{\mathrm{xc}}^{\mathrm{SAOP}}$ is tested for the prototype molecules CO, N_2, CH_2O, and C_2H_4. These molecules have been selected because accurate reference values are available for the excitation energies and other response properties [although the (hyper)polarizabilities of formaldehyde seem to form an exception], and because they have been employed in other TDDFPT benchmark studies,[4,5] which facilitates a comparison to the performance of the most popular functionals. A wide spectrum of linear and nonlinear response properties for CO, N_2, and C_2H_4 as well as excitation energies of the CH_2O molecule are calculated with $\nu_{\mathrm{xc}}^{\mathrm{SAOP}}$. The new potential provides high quality results for all the calculated static and frequency-dependent molecular response properties and a substantial improvement upon the LDA, GGA, and LB potentials. In Sec. V the conclusions are drawn and prospects of further improving of $\nu_{\mathrm{xc}}^{\mathrm{SAOP}}$ are discussed.

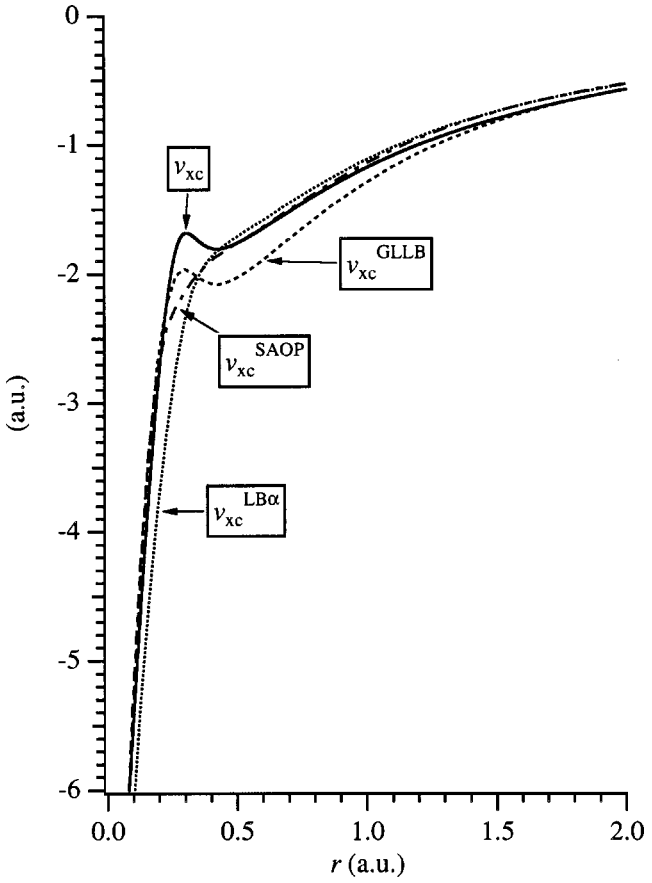

FIG. 1. A comparison of the SAOP, LBα, and GLLB potentials with the accurate v_{xc} for the Ne atom.

II. STATISTICAL AVERAGE OF ORBITAL POTENTIALS

The use of the statistical average of orbital potentials (SAOP)[36] is motivated by the need for a flexible scheme to build model potentials that have known, desirable features both asymptotically and in the inner region. We will exploit the recent development of the LB and GLLB model potentials,[34,37,38] which approximate the accurate potential v_{xc} closely either in the outer (LB), or in the inner (GLLB) regions of molecules.

The LB potential[34] reproduces the Coulombic asymptotics of v_{xc} in the outer region. In this paper we use a modified LB potential $v_{xc}^{LB\alpha}(\alpha,\beta;\mathbf{r})$, which contains two empirical parameters α and β and which can be written in the form

$$v_{xc\sigma}^{LB\alpha}(\alpha,\beta;\mathbf{r})=\alpha v_{x\sigma}^{LDA}(\mathbf{r})+v_{c\sigma}^{LDA}(\mathbf{r}) - \frac{\beta x_\sigma^2(\mathbf{r})\rho_\sigma^{1/3}(\mathbf{r})}{1+3\beta x_\sigma(\mathbf{r})\ln\{x_\sigma(\mathbf{r})+[x_\sigma^2(\mathbf{r})+1]^{1/2}\}}, \tag{2.1}$$

where $\rho_\sigma(\mathbf{r})$ is the density of electrons with spin σ, while $v_{x\sigma}^{LDA}$ and $v_{c\sigma}^{LDA}$ are the LDA exchange and correlation potentials. The last term in (2.1) is the gradient correction with $x_\sigma(\mathbf{r})=|\nabla\rho_\sigma(\mathbf{r})|[\rho_\sigma(\mathbf{r})]^{-4/3}$, which ensures the proper asymptotics $v_{xc\sigma}^{LB\alpha}(\mathbf{r})\to -1/r$, $r\to\infty$ for an exponentially decaying density and which has the same functional form as the Becke correction for the exchange energy density.[39]

Figure 1 compares for the Ne atom $v_{xc}^{LB\alpha}$ (with $\alpha=1.19$ and $\beta=0.01$) with the essentially accurate v_{xc} generated from *ab initio* ρ.[40] Indeed, $v_{xc}^{LB\alpha}$ goes close to v_{xc} in the outer region $r>0.5$ a.u., but it substantially overestimates exchange and correlation in the inner region. Note that the performance of the original LB potential agrees with this illustration. LB performs better than LDA or GGA for (hyper)polarizabilities and higher excitation energies, which depend primarily on the quality of the potential in the outer region. On the other hand, for the lowest excitations, dipole moments and equilibrium geometries, which are also sensitive to the form of the potential in the inner region, the LB potential does not perform particularly well, the LDA and GGA potentials seem to be preferable in many cases.

The behavior of the v_{xc} potential in the inner region has been recently modeled with the GLLB potential v_{xc}^{GLLB}.[37,38] This potential reproduces the atomic shell structure in the inner regions, which is characterized by different slopes of the potential in different shells, and a little peak in the intershell regions. These features of the exact v_{xc} originate from the physics of electron exchange and correlation. It has proven helpful to separate the exchange-correlation potential in a hole part, which is just the potential of the XC hole $\bar{v}_{xc\sigma}^{hole}$ dependent on the pair correlation function $\bar{g}(\mathbf{r}_1,\mathbf{r}_2)$ integrated over the coupling constant λ of the electron–electron interaction λ/r_{12}), and a so-called ''response'' part, which contains the functional derivative of the (λ-integrated) pair correlation function $\bar{g}(\mathbf{r}_1,\mathbf{r}_2)$. The response potential has a very characteristic stepped form, which builds in the intershell peaks in the total v_{xc}. v_{xc}^{GLLB} consists of a term modeling $\bar{v}_{xc\sigma}^{hole}$ and a term representing the response potential $v_{resp\sigma}$,

$$v_{xc\sigma}^{GLLB}(\mathbf{r})=\bar{v}_{xc\sigma}^{hole}(\mathbf{r})+v_{resp\sigma}(\mathbf{r}). \tag{2.2}$$

The potential $\bar{v}_{xc\sigma}^{hole}$ is approximated within $v_{xc\sigma}^{GLLB}$ as twice the exchange-correlation energy density $\epsilon_{xc\sigma}^{GGA}$ of the GGA, which is the sum of the exchange energy density $\epsilon_{x\sigma}^{B}(\rho_\sigma,x_\sigma;\mathbf{r})$ of Becke[39] and the correlation energy density $\epsilon_c^{PW}(\rho,x,\xi;\mathbf{r})$ of Perdew and Wang,[41–43]

$$\bar{v}_{xc\sigma}^{hole}(\mathbf{r})=2\epsilon_{xc\sigma}^{GGA}(\mathbf{r})=2\epsilon_{x\sigma}^{B}(\rho_\sigma,x_\sigma;\mathbf{r})+2\epsilon_c^{PW}(\rho,x,\xi;\mathbf{r}), \tag{2.3}$$

$$E_x^B=\sum_\sigma \int \rho_\sigma(\mathbf{r})\epsilon_{x\sigma}^{B}(\rho_\sigma,x_\sigma;\mathbf{r})d\mathbf{r}, \tag{2.4}$$

$$E_c^{PW}=\int \rho(\mathbf{r})\epsilon_c^{PW}(\rho,x,\xi;\mathbf{r})d\mathbf{r}, \tag{2.5}$$

where ξ is the local spin-polarization. The characteristic stepped form of $v_{resp\sigma}$,[44] reflecting the atomic shell structure in the inner regions, is represented with the model potential

$$v_{resp\sigma}(\mathbf{r})=K_\sigma\sum_i^{N_\sigma}\sqrt{\epsilon_{N\sigma}-\epsilon_{i\sigma}}\frac{|\psi_{i\sigma}(\mathbf{r})|^2}{\rho_\sigma(\mathbf{r})}, \tag{2.6}$$

$\epsilon_{i\sigma}$ and $\epsilon_{N\sigma}$ are the energies of a given occupied orbital $\psi_{i\sigma}$ and the highest occupied orbital $\psi_{N\sigma}$, respectively. The potential (2.6) approximates the response part $v_{resp\sigma}^{KLI}$ of the Krieger–Li–Iafrate (KLI) potential,[45]

$$\nu_{\mathrm{resp}\sigma}(\mathbf{r})=\sum_{i}^{N_\sigma} w_i \frac{|\psi_{i\sigma}(\mathbf{r})|^2}{\rho_\sigma(\mathbf{r})}, \tag{2.7}$$

where the weights w_i are expressed via one- and two-electron integrals over $\{\psi_{i\sigma}\}$. The reasons for choosing $K_\sigma\sqrt{\epsilon_{N\sigma}-\epsilon_{i\sigma}}$ as an approximation to the KLI weights w_i are given in Ref. 37. In this paper the parameter $K_\sigma=0.42$ is used, which is a reasonable value, as it is in between the value $K=0.382$ derived for (2.6) from the electron gas model,[37] and the value $K=0.47$ from a fit to atomic data.[38]

Figure 1 compares $\nu_{\mathrm{xc}}^{\mathrm{GLLB}}$ with the accurate ν_{xc} and $\nu_{\mathrm{xc}}^{\mathrm{LB}\alpha}$ for the Ne atom. Indeed, $\nu_{\mathrm{xc}}^{\mathrm{GLLB}}$ reproduces (though with some displacement) the intershell peak of ν_{xc} at $r\approx 0.3\,a.e.$ and it goes close to ν_{xc} at smaller r. However, $\nu_{\mathrm{xc}}^{\mathrm{GLLB}}$ differs considerably from ν_{xc} in the outer region $0.3<r<1.5$ a.u. The deficiency of $\nu_{\mathrm{xc}}^{\mathrm{GLLB}}$ in the outer region is responsible for the consistent underestimation of the molecular polarizabilities calculated with this potential.[13]

The main idea of the SAOP[36] is to combine $\nu_{\mathrm{xc}}^{\mathrm{LB}\alpha}$ and $\nu_{\mathrm{xc}}^{\mathrm{GLLB}}$ in such a way that the resulting potential $\nu_{\mathrm{xc}}^{\mathrm{SAOP}}$ would be close to $\nu_{\mathrm{xc}}^{\mathrm{LB}\alpha}$ in the outer region and close to $\nu_{\mathrm{xc}}^{\mathrm{GLLB}}$ in the inner region, thus providing a balanced approximation to ν_{xc} in all regions. It is, of course, desirable to combine $\nu_{\mathrm{xc}}^{\mathrm{LB}\alpha}$ and $\nu_{\mathrm{xc}}^{\mathrm{GLLB}}$ in a smooth way, which allows us to represent the combination with the analytical formula. This can be achieved with the statistical average of different model orbital potentials $\nu_{\mathrm{xc}i\sigma}^{\mathrm{mod}}(\mathbf{r})$ for the occupied orbitals $\psi_{i\sigma}(\mathbf{r})$,

$$\nu_{\mathrm{xc}\sigma}^{\mathrm{SAOP}}(\mathbf{r})=\sum_{i=1}^{N_\sigma} \nu_{\mathrm{xc}i\sigma}^{\mathrm{mod}}(\mathbf{r})\,\frac{|\psi_{i\sigma}(\mathbf{r})|^2}{\rho_\sigma(\mathbf{r})}, \tag{2.8}$$

where individual orbital potentials $\nu_{\mathrm{xc}i\sigma}^{\mathrm{mod}}(\mathbf{r})$ are obtained with the following exponential interpolation between $\nu_{\mathrm{xc}\sigma}^{\mathrm{LB}\alpha}$ and $\nu_{\mathrm{xc}\sigma}^{\mathrm{GLLB}}$,

$$\nu_{\mathrm{xc}i\sigma}^{\mathrm{mod}}(\mathbf{r})=\exp[-2(\epsilon_{N\sigma}-\epsilon_{i\sigma})^2]\,\nu_{\mathrm{xc}\sigma}^{\mathrm{LB}\alpha}(\mathbf{r}) + \{1-\exp[-2(\epsilon_{N\sigma}-\epsilon_{i\sigma})^2]\}\,\nu_{\mathrm{xc}\sigma}^{\mathrm{GLLB}}(\mathbf{r}). \tag{2.9}$$

For $\psi_{N\sigma}$, Eq. (2.9) reduces to $\nu_{\mathrm{xc}\sigma}^{\mathrm{LB}\alpha}$ and for close-lying orbitals $\psi_{i\sigma}$ with small relative energy $(\epsilon_{N\sigma}-\epsilon_{i\sigma})$ the potential $\nu_{\mathrm{xc}i\sigma}^{\mathrm{mod}}$ remains close to $\nu_{\mathrm{xc}\sigma}^{\mathrm{LB}\alpha}$. On the other hand, for the subvalence and core orbitals with large $(\epsilon_{N\sigma}-\epsilon_{i\sigma})$ the potential $\nu_{\mathrm{xc}i\sigma}^{\mathrm{mod}}$ reduces to $\nu_{\mathrm{xc}\sigma}^{\mathrm{GLLB}}$. The choice of the orbital energy difference $(\epsilon_{N\sigma}-\epsilon_{i\sigma})$ as the interpolation argument preserves the important gauge invariance requirement on the XC potential, according to which the addition of a constant to an external potential should not alter ν_{xc}. Upon this addition, both orbital energies $\epsilon_{i\sigma}$ and $\epsilon_{N\sigma}$ are shifted by the constant, however, their difference remains unaltered, so that $\nu_{\mathrm{xc}i\sigma}^{\mathrm{mod}}$ and $\nu_{\mathrm{xc}\sigma}^{\mathrm{SAOP}}$ do not change.

SAOP is based on the fact that the statistical weight $|\psi_{i\sigma}(\mathbf{r})|^2/\rho_\sigma(\mathbf{r})$ of the orbital $\psi_{i\sigma}(\mathbf{r})$ is close to one in the region of its localization and decays rapidly to zero outside this region, so that $\nu_{\mathrm{xc}\sigma}^{\mathrm{SAOP}}$ is close in this region to the corresponding individual potential $\nu_{\mathrm{xc}i\sigma}^{\mathrm{mod}}$. This means that in the inner region with the dominance of core and subvalence orbitals $\nu_{\mathrm{xc}\sigma}^{\mathrm{SAOP}}$ is close to $\nu_{\mathrm{xc}\sigma}^{\mathrm{GLLB}}$, while in the outer region with the prevailing higher-lying orbitals $\nu_{\mathrm{xc}\sigma}^{\mathrm{SAOP}}$ is close to $\nu_{\mathrm{xc}\sigma}^{\mathrm{LB}\alpha}$, thus providing a balanced approximation to the exact ν_{xc}. Figure 1 confirms this expectation. One can see that $\nu_{\mathrm{xc}}^{\mathrm{SAOP}}$ reproduces very well the atomic shell slopes of the accurate ν_{xc} in both inner and outer regions and it goes close to ν_{xc} everywhere, with the only exception of the intershell peak region. However, as was argued elsewhere,[45] the peak does not seem to be an important feature of the XC potential to reproduce in order to have good orbital and global energy characteristics.

In this paper the parameters $\alpha=1.19$ and $\beta=0.01$ are used for the LBα part of the SAOP potential, which were fitted to reproduce the excitation energies and the dipole polarizabilities (see Sec. IV). This new β value of 0.01 is, in fact, much closer to twice Becke's value ($2\beta_{\mathrm{Becke}}=0.0086$) than the original LB value of $\beta_{\mathrm{LB}}=0.05$ (β_B is doubled, since here we consider not the energy density with correct asymptotic behavior of $-1/2r$, but rather the potential of the exchange hole which should display a $-1/r$ behavior for large r). The empirical effect of choosing α of the LBα, which is larger than $\alpha=1.0$ of LDA, is similar to a rigid downward shift of the LDA potential in the inner region for the asymptotically corrected LDA model.[35] The results of the calculations with the SAOP potential will be presented in Sec. IV.

In the end of this section we would like to delineate briefly the differences between the SAOP approach presented in this section and the asymptotical corrections to the LDA[35] and GGA[5] potentials. Both Refs. 35 and 5 use a shift of a part of the model ν_{xc} by the constant $(I_p+\epsilon_{N\sigma})$, where I_p is the ionization potential which should be pre-calculated with a standard ΔSCF GGA calculations. Thus, each response calculation requires two additional GGA calculations: one for the N-electron system and one for the $(N-1)$-electron system. In contrast to this, no knowledge of I_p is required for the construction of $\nu_{\mathrm{xc}\sigma}^{\mathrm{SAOP}}$ of (2.1).

Both Refs. 35 and 5 use in the inner region a potential, which is a functional derivative of the LDA/GGA XC energy functional, while at the long-range asymptotics they employ potentials with a different analytical representation. As a result, the asymptotically corrected LDA potential of Ref. 35 possesses a discontinuity in its derivative. The asymptotically corrected GGA potential of Ref. 5 also lacks a common analytical representation for the inner and outer regions and it is defined on a grid. For an atom, the asymptotical correction produces a smooth potential, while for a molecule the potential constructed in Ref. 5 may well have discontinuities at the borders of the inner and outer regions with the intermediate region. Contrary to this, the present SAOP directly approximates the Kohn–Sham XC potential, so that neither the LBα, nor the GLLB parts are the explicit functional derivatives of some approximate XC energy functional. One can hope that such a direct modeling of the XC potential could be especially successful in TDDFPT, where the proper form of the potential is all important. The resulting $\nu_{\mathrm{xc}\sigma}^{\mathrm{SAOP}}$ is a smooth potential which has the unique analytical representation (2.1)–(2.8). In both Refs. 35 and 5 the corrections are made well in the region of the density tails, while the SAOP (2.1),(2.2) switches from $\nu_{\mathrm{xc}\sigma}^{\mathrm{inner}}$ to $\nu_{\mathrm{xc}\sigma}^{\mathrm{outer}}$ in the valence region with the typical orbital energy $\epsilon_{i\sigma}=-1.4$ Hartree. Note, finally, that both models Ref. 35 and Ref. 5 are designed to incorporate effectively the particle number discontinuity of

the exact ν_{xc},[46] while the present SAOP potential possesses the particle number discontinuity in a natural way, through its steplike response part (2.6).[47,48]

III. DETAILS OF THE RESPONSE CALCULATIONS

Time-dependent density functional perturbation theory (TDDFPT) has been thoroughly analyzed and discussed in the literature,[1,2,49] so that only the basic formulas of the calculated response properties are presented below. The components of the dipole polarizability α_{ab} and hyperpolarizability β_{abc} and γ_{abcd} tensors can be defined through an expansion of the dipole moment μ_a into different orders of the external fields E^b (the indices $ab\ldots$ label the Cartesian axes x,y,z),

$$\mu_a=\mu_a(E=0)+\sum_b \alpha_{ab}E^b+\frac{1}{2!}\sum_{bc}\beta_{abc}E^bE^c + \frac{1}{3!}\sum_{bcd}\gamma_{abcd}E^bE^cE^d+\cdots. \tag{3.1}$$

These tensors with their dependence on the frequency ω_b of the applied electric field can be obtained from the trace of the dipole moment matrix μ_a and the matrices $P^{(n)}$ of the expansion of the electron density P in nth order of the field

$$\alpha_{ab}(-\omega_\sigma;\omega_b)=-\mathrm{Tr}[\mu_a P^b(\omega_b)], \tag{3.2}$$

$$\beta_{abc}(-\omega_\sigma;\omega_b,\omega_c)=-\mathrm{Tr}[\mu_a P^{bc}(\omega_b,\omega_c)], \tag{3.3}$$

$$\gamma_{abcd}(-\omega_\sigma;\omega_b,\omega_c,\omega_d)=-\mathrm{Tr}[\mu_a P^{bcd}(\omega_b,\omega_c,\omega_d)], \tag{3.4}$$

$$P=P^{(0)}+\sum_a P^aE^a+\frac{1}{2!}\sum_{ab}P^{ab}E^aE^b + \frac{1}{3!}\sum_{abc}P^{abc}E^aE^bE^c+\cdots, \tag{3.5}$$

where ω_σ is the sum frequency $\omega_\sigma=\omega_b+\omega_c+\cdots$. In the actual calculation, γ is obtained from a finite field calculation of β,[18,19,21] which is calculated analytically. The trace on the right-hand side of Eq. (3.3) is rewritten such that only first-order quantities remain, which avoids the need of solving second-order response equations for the second-order density matrix. The isotropic C_6 van der Waals dispersion coefficient governs the isotropic long-range $-1/R^6$ induced dipole-induced dipole attraction between molecules. For the case of two identical systems it is calculated from the average dipole polarizability of the monomer at imaginary frequencies $\alpha_d(i\omega)$

$$C_6=\frac{3}{\pi}\int_0^\infty \alpha_d^2(i\omega)d\omega. \tag{3.6}$$

The S_{-4} and S_{-6} Cauchy coefficients relate to the frequency dispersion in the average dipole polarizability $\alpha_d(\omega)$,

$$\alpha_d(\omega)=\alpha_d(0)+S_{-4}\omega^2+S_{-6}\omega^4+\cdots. \tag{3.7}$$

They are calculated from all oscillator strengths f_i, weighed by an even power of the excitation energies ω_i,

$$S_{-2k}=\sum_i \omega_i^{-2k}f_i. \tag{3.8}$$

The excitation energies and oscillator strengths are obtained from the solution of the following eigenvalue problem.[2,9]

$$\Omega\mathbf{F}_i=\omega_i^2\mathbf{F}_i, \tag{3.9}$$

where the components of the matrix Ω are given by

$$\Omega_{ia\sigma,jb\tau}=\delta_{\sigma\tau}\delta_{ij}\delta_{ab}(\epsilon_{a\sigma}-\epsilon_{i\sigma})^2 + 2\sqrt{(\epsilon_{a\sigma}-\epsilon_{i\sigma})}K_{ia\sigma,jb\tau}\sqrt{(\epsilon_{b\sigma}-\epsilon_{j\sigma})}. \tag{3.10}$$

In (3.10), $\epsilon_{i\sigma}$ and $\epsilon_{j\sigma}$ are the energies of the occupied KS orbitals $\psi_{i\sigma}$ and $\psi_{j\sigma}$ in (1.1), while $\epsilon_{a\sigma}$ and $\epsilon_{b\sigma}$ are the energies of the virtual orbitals $\psi_{a\sigma}$ and $\psi_{b\sigma}$. The elements $K_{ia\sigma,jb\tau}$ of the coupling matrix consist of the Hartree and exchange-correlation parts,

$$K_{ia\sigma,jb\tau}=K^{\mathrm{H}}_{ia\sigma,jb\tau}+K^{\mathrm{xc}}_{ia\sigma,jb\tau}, \tag{3.11}$$

$$K^{\mathrm{H}}_{ia\sigma,jb\tau}=\int d\mathbf{r}\int d\mathbf{r}'\ \psi_{i\sigma}(\mathbf{r})\psi_{a\sigma}(\mathbf{r}) \times\frac{1}{|\mathbf{r}-\mathbf{r}'|}\psi_{j\tau}(\mathbf{r}')\psi_{b\tau}(\mathbf{r}'), \tag{3.12}$$

$$K^{\mathrm{xc}}_{ia\sigma,jb\tau}=\int d\mathbf{r}\int d\mathbf{r}'\ \psi_{i\sigma}(\mathbf{r})\psi_{a\sigma}(\mathbf{r})f^{\sigma\tau}_{\mathrm{xc}}(\mathbf{r},\mathbf{r}',\omega) \times\psi_{j\tau}(\mathbf{r}')\psi_{b\tau}(\mathbf{r}') \tag{3.13}$$

(real orbitals are considered). The desired excitation energies are equal to ω_i, and the oscillator strengths are obtained from the eigenvectors $\mathbf{F}_i$.[2]

The technical aspects of the solution of all these equations are to be found in Refs. 6,49. As in our previous calculations,[3,13,21] we used the RESPONSE module of the Amsterdam density functional program (ADF). We have attempted to get answers close to the basis set limit for the experimental geometries (the actual basis sets and geometries are available online [cite http://tc.chem.vu.nl/~vgisberg/saop.calcs]). We have used strict criteria for the numerical integration accuracy and the convergence of the SCF cycles, so that the resulting errors can be assumed negligible. The choice of basis sets for the calculations below is a more difficult point. It is well known that large basis sets are required for near-basis-set-limit quality calculations on such properties as hyperpolarizabilities and high-lying excitation energies. However, although many of such basis sets are commonly available for Gaussian orbital based programs, this is not the case for the Slater type orbitals used in our calculations with the ADF program. We therefore added increasing numbers of diffuse functions to the standard STO basis sets available for the ADF package. Too many diffuse functions on all atoms lead to numerical problems, however, because of the danger of near linear dependence. We have checked that a good balance was obtained between numerical stability and large basis sets, by removing of nearly linear-dependent combinations of diffuse atomic orbitals. Typically, four of such combinations had to be removed for the basis sets we used. From a comparison with other basis sets (both smaller and larger) we can be confident that our final results are reliable. For N_2 and CO the basis sets were even slightly larger than those used in our previous work,[21] while the size of the basis sets for other molecules is com-

TABLE I. Vertical excitation energies (eV) and other response properties (a.u.) of CO.

Excited state and transition	LDA	LB	LBα	SAOP	Expt./Ref.[a]
$^3\Pi,\sigma\rightarrow\pi^*$	5.96	5.54	5.72	6.28	6.32
$^3\Sigma^+,\pi\rightarrow\pi^*$	8.41	8.38	8.42	8.64	8.51
$^1\Pi,\sigma\rightarrow\pi^*$	8.17	7.92	8.12	8.56	8.51
$^3\Delta,\pi\rightarrow\pi^*$	9.18	9.17	9.21	9.37	9.36
$^3\Sigma^-,\pi\rightarrow\pi^*$	9.87	9.88	9.92	10.03	9.88
$^1\Sigma^-,\pi\rightarrow\pi^*$	9.87	9.88	9.92	10.03	9.88
$^1\Delta,\pi\rightarrow\pi^*$	9.19	10.35	10.38	10.46	10.23
$^3\Sigma^+,\sigma\rightarrow 3s$	8.99	10.69	10.41	10.32	10.4
$^1\Sigma^+,\sigma\rightarrow 3s$	8.85	11.01	10.71	10.69	10.78
$^3\Sigma^+,\sigma\rightarrow 3p\sigma$	9.18	11.77	11.40	11.26	11.3
$^1\Sigma^+,\sigma\rightarrow 3p\sigma$	9.18	11.75	11.44	11.41	11.40
$^1\Pi,\sigma\rightarrow 3p\pi$	9.19	12.02	11.64	11.58	11.53
$^3\Pi,\sigma\rightarrow 3p\pi$	9.19	11.33	11.50	11.51	11.55
$^1\Sigma^+,\sigma\rightarrow 3d\sigma$	9.19	13.04	12.65	12.59	12.4
Av. error	1.26	0.32	0.15	0.09	
α_d	13.70	12.65	12.63	13.02	13.08
S_{-4}	57.21	48.85	48.87	48.58	48.27
S_{-6}	393.0	332.4	323.1	291.7	296.5
C_6	83.95	75.18	74.49	79.02	81.31
α_q	125.03	108.99	107.47	112.62	110.24
					112.1
$\beta_\parallel$	30.45	20.85	22.08	23.80	26.6
β_{SHG}	36.61	23.65	25.36	27.58	29.9 ($\pm$3.2)
$\gamma_\parallel$	2246	1185	1268	1358	1475
γEFISH	2957	1439	1561	1679	1720 ($\pm$48)

[a]See Sec. IV for the sources of the experimental and other reference data.

TABLE II. Vertical excitation energies (eV) and other response properties (a.u.) of N_2.

Excited state and transition	LDA	LB	LBα	SAOP	Expt./Ref.[a]
$^3\Sigma_u^+,\pi_u\rightarrow\pi_g$	7.90	7.53	7.61	7.89	7.75
$^3\Pi_g,\sigma_g\rightarrow\pi_g$	7.58	7.21	7.47	7.81	8.04
$^3\Delta_u,\pi_u\rightarrow\pi_g$	8.84	8.53	8.61	8.82	8.88
$^1\Pi_g,\sigma_g\rightarrow\pi_g$	9.07	8.71	9.00	9.31	9.31
$^3\Sigma_u^-,\pi_u\rightarrow\pi_g$	9.68	9.42	9.50	9.66	9.67
$^1\Sigma_u^-,\pi_u\rightarrow\pi_g$	9.68	9.42	9.50	9.66	9.92
$^1\Delta_u,\pi_u\rightarrow\pi_g$	10.23	10.00	10.08	10.21	10.27
$^3\Pi_u,\sigma_u\rightarrow\pi_g$	10.37	10.10	10.25	10.88	11.19
$^3\Sigma_g^+,\sigma_g\rightarrow 3s\sigma_g$	10.32	12.27	12.03	11.80	12.0
$^1\Sigma_g^+,\sigma_g\rightarrow 3s\sigma_g$	9.70	12.26	12.20	12.20	12.20
$^1\Pi_u,\sigma_g\rightarrow 3p\pi_u$	10.53	12.86	13.00	12.45	12.90
$^1\Sigma_u^+,\sigma_g\rightarrow 3p\sigma_u$	10.43	13.46	13.13	12.86	12.98
$^1\Pi_u,\pi_u\rightarrow 3s\sigma_g$	10.60	13.51	13.16	13.17	13.24
$^1\Pi_u,\sigma_u\rightarrow\pi_g$	10.99	14.06	13.60	13.58	13.63
$^1\Sigma_u^+,\ldots$	10.51	14.26	14.16	14.07	14.25
Av. error	1.34	0.38	0.23	0.11	
α_d	12.27	11.49	11.43	11.82	11.74
S_{-4}	34.45	29.21	29.38	30.45	30.11
S_{-6}	129.4	96.7	98.5	101.6	101.8
C_6	76.91	70.28	69.35	73.67	73.42
α_q	95.11	83.91	82.12	85.85	78.2
					80.7
$\gamma_\parallel$	1430.1	768.5	816.4	895.1	1010
γEFISH	1731.3	879.0	941.1	1037.6	1058$\pm$6, 1030$\pm$12

[a]See Sec. IV for the sources of the experimental and other reference data.

parable. In all cases, small deviations from our previous results may occur, due to differences in the basis sets.

The SAOP potential of Eqs. (2.1)–(2.8) has been compared with the LDA, LB, LBα potentials and in all calculations the adiabatic LDA (ALDA) XC kernels f_{xc} and g_{xc}[9,21] have been used. All properties have been calculated analytically, except for the second hyperpolarizabilities γ, which have been obtained from the same finite field procedure as in Refs. 18,19,21. We have also calculated average hyperpolarizabilities for those nonlinear optical (NLO) effects for which reliable experimental data are available, such as second harmonic generation (SHG) [$\beta(-2\omega;\omega,\omega)$ or βSHG] and electric field-induced second harmonic generation (EFISH) [$\gamma(-2\omega;\omega,\omega,0)$ or γEFISH] at the experimental fundamental laser wavelength of 694.3 nm. The results of the calculations are presented in the next section.

IV. MOLECULAR RESPONSE PROPERTIES

Tables I–IV compare a variety of response properties for the prototype molecules CO, N_2, CH_2O, and C_2H_4 calculated within TDDFPT with the SAOP, LDA, LB, LBα potentials and with the ALDA XC kernels f_{xc} and g_{xc}. We start with the comparison of the calculated and experimental vertical excitation energies ω_i, the latter are taken from[5] for CO and N_2 and from Ref. 50 for C_2H_4 and CH_2O. For the latter molecule the experimental situation is not completely unambiguous, and we conform to the choice of Ref. 50. In all cases LDA with its deficient long-range asymptotics yields a reasonable estimate only for ω_i lower than the LDA ionization energy,[8] $\omega_i<I_p^{\mathrm{LDA}}=-\epsilon_{N\sigma}^{\mathrm{LDA}}$, the latter being substantially lower (in absolute value) than the corresponding experimental I_p value. For higher excitations LDA is not reliable and it completely fails to predict both the values and the order of the excitations. Note that the average absolute error of LDA for C_2H_4 is smaller than for other molecules.

The latter trend is reversed for other methods considered. For N_2, CO, and CH_2O LB yields a reasonable estimate of higher excitations, which is further improved with LBα (See Tables I–III). Already LBα provides a good overall quality with small average errors of the calculated ω_i. However, both LB and LBα do not definitely improve the lowest excitations (in fact they are worse than LDA for several low-lying excitation energies). Improvement for the important low-lying excitations is accomplished only by the

TABLE III. Vertical excitation energies (eV) of CH_2O.

Excited state and transition	LDA	LB	LBα	SAOP	Expt.[a]
$^3A_2,n\rightarrow\pi^*$	3.08	2.93	3.10	3.64	3.5
$^1A_2,n\rightarrow\pi^*$	3.69	3.55	3.72	4.24	4.1
$^3A_1,\pi\rightarrow\pi^*$	6.20	6.03	6.08	6.33	6.0
$^3B_2,n\rightarrow 3s$	5.79	7.08	6.85	6.92	7.09
$^1B_2,n\rightarrow 3s$	5.85	7.38	7.07	7.14	7.13
$^3B_2,n\rightarrow 3p_{a1}$	6.61	8.33	8.05	8.08	7.92
$^1B_2,n\rightarrow 3p_{a1}$	6.57	8.49	8.17	8.21	7.98
$^3A_1,n\rightarrow 3p_{b2}$	6.58	8.39	8.09	8.15	8.11
$^1A_1,n\rightarrow 3p_{b2}$	6.54	8.61	8.22	8.26	8.14
$^1B_1,\sigma\rightarrow\pi^*$	7.29	8.45	8.75	9.01	9.0
Av. error	1.12	0.36	0.18	0.14	

[a]The experimental excitation energies are taken from Ref. 50.

TABLE IV. Vertical excitation energies (eV, all excitations are from the π-orbital) and other response properties (a.u.) of C_2H_4. The *z*-axis is along the C═C bond; the *x*-axis is perpendicular to the molecular plane.

Excited state and orbital	LDA	LB	LBα	SAOP	Expt./Ref.[a]
$^3B_{1u}, \pi^*$	4.63	4.38	4.43	4.64	4.36
$^3B_{3u}$,3*s*	6.55	7.58	7.22	7.18	6.98
$^1B_{3u}$,3*s*	6.59	7.74	7.35	7.29	7.15
$^1B_{1u}, \pi^*$	7.36	7.62	7.60	7.62	7.66
$^3B_{1g}$,3p_y	7.03	8.29	7.92	7.91	7.79
$^3B_{2g}$,3p_z	7.00	8.29	7.87	7.81	7.79
$^1B_{1g}$,3p_y	7.03	8.41	8.01	8.00	7.83
$^1B_{2g}$,3p_z	7.02	8.45	8.01	7.94	8.0
^3A_g,3p_x	7.26	9.28	8.81	8.70	8.15
^1A_g,3p_x	7.28	9.54	9.03	8.91	8.29
$^3B_{3u}$,3d_z2	7.29	9.47	9.07	8.96	8.57
$^1B_{3u}$,3d_z2	7.31	9.56	9.12	9.03	8.62
Av. error	0.78	0.63	0.28	0.25	
α_d	28.72	27.65	27.43	27.96	27.70
S_{-4}	165.3	140.9	144.7	148.0	143.5
S_{-6}	1549	1134	1218	1244	1202
$\gamma_\parallel$	8900	4500	5100	5500	6700
γEFISH	14000	6100	7200	7900	9030±200

[a]See Sec. IV for the sources of the experimental and other reference data.

SAOP. It is the replacement within the SAOP [Eqs. (2.1)] of LBα [Eq. (2.3)] with GLLB [Eq. (2.4)] in the inner regions, which is responsible for the displayed high quality of the lowest excitations calculated with SAOP. The latter reproduces very well both lower and higher experimental excitation energies for all three molecules and the average errors of SAOP approach the benchmark accuracy of 0.1 eV for the electronic spectra.

For C_2H_4, however, LB overcorrects: While LDA underestimates higher excitations, LB considerably overestimates them (see Table IV). This correlates with the fact that for ethylene the LB ionization energy $I_p^{\mathrm{LB}} = -\epsilon_{N\sigma}^{\mathrm{LB}} = 11.85$ eV is considerably higher than the experimental value $I_p = 10.51$ eV. Because of this, the average LB error in this case is only somewhat lower than the LDA error. LBα partially corrects this error and SAOP produces the lowest average error of 0.25 eV, which is still higher than those for the other three molecules. Since its main source are the highest excitations, starting from the ^3A_g state at 8.70 eV (LBα 8.81, exp 8.15) upward, we hope to improve the performance of the SAOP potential further by correcting its far asymptotics as discussed in Sec. V.

If we look at the high-lying excitations of C_2H_4 more closely, we note that the energies of the singlet and triplet B_{3u} excitations associated with the $3d_z2$ orbital are quite close to each other (8.62 vs 8.57 eV in the experiment and 9.03 vs 8.96 eV with the SAOP). The associated orbital energy difference for these transitions is 9.039 eV, implying that the Hartree and exchange-correlation elements of the coupling matrix **K** [Eqs. (3.11)–(3.13)] produce very small corrections to the simple KS orbital energy difference approximation to the excitation energy. This is consistent with the analysis of the results obtained with the exact ν_{xc} for the He and Be atoms[51] (see also Ref. 52). As was shown in Ref. 51, the KS orbital energy differences are already very good approximations to the excitation energies from the highest occupied molecular orbital to the Rydberg levels. The numbers in Table IV seem to suggest that the KS orbital energies should behave similarly for the high-lying Rydberg-like excitation energies here. This fact provides another strong indication that further improvement of the potential at far asymptotics is needed in this case. This should bring down the orbital energy differences for excitations to the high-lying virtual orbitals. High-lying excitations like these, which should be very close to the KS orbital energy differences, can also be used for a rapid judgement of the quality of approximate potentials in this outer region.

We proceed with the discussion of the static response properties, namely, the average dipole α_d and quadrupole α_q polarizabilities and the first and second average hyperpolarizabilities $\beta_\parallel$ and $\gamma_\parallel$. The experimental/reference values for α_d are taken from Ref. 3, the reference α_q are taken from Ref. 14, and the reference $\beta_\parallel$ and $\gamma_\parallel$ are taken from.[21] LDA makes molecules artificially more polarizable, so that it consistently overestimates all above-mentioned quantities for the molecules considered here. This is understandable, since the potential $\nu_{\mathrm{xc}}^{\mathrm{LDA}}$ is not attractive enough, especially in the outer regions. From this point of view, as far as α_d, $\beta_\parallel$, and $\gamma_\parallel$ are concerned, both LB and LBα potentials are overattractive, since they consistently underestimate these quantities (the LB and LBα α_q values do not display such a definite trend). The SAOP approach provides the desired balance. As a rule, the SAOP static polarizabilities and hyperpolarizabilities are in between the corresponding LDA and LB LBα values (see Tables I and II). In all cases SAOP displays the best agreement with the reference data (for example, the errors in the average dipole polarizabilities are less than 1% for CO, N_2, and C_2H_4, with the only exception of α_q for N_2, for which the LB and LBα values are somewhat better.

The SAOP ω_i and α_d values are of a comparable accuracy with those obtained with the asymptotically corrected GGA potential HCTH-AC,[5] the overall best DFT results thus far. In the case of CO and N_2 the average ω_i errors of SAOP of 0.09 and 0.11 eV, respectively, are definitely lower than the corresponding errors of 0.32 and 0.34 eV of HTCH-AC. The trend is reversed for C_2H_4 with an error of 0.25 eV for SAOP and 0.07 eV for HCTH-AC, which might be an indication that the outer region of this molecule is more accurately described by the Fermi–Amaldi potential than by the LB potential. However, the polarizability $\alpha_{\mathrm{a}\nu} = 27.96$ a.u. obtained for C_2H_4 with SAOP (see Table IV) is definitely closer to the experimental value $\alpha_{\mathrm{a}\nu} = 27.70$ a.u. than $\alpha_{\mathrm{a}\nu} = 27.11$ a.u. obtained with HCTH-AC. Theoretical virtues of the SAOP and the differences between SAOP and HCTH-AC have been discussed in Sec. II.

Several frequency-dependent quantities are presented in Tables I, II, and IV for CO, N_2, and C_2H_4. The semiempirical C_6 coefficients are taken from Ref. 3, the experimental and reference β and γ values are taken from Ref. 21, the empirical S_{-4} and S_{-6} coefficients are taken from Ref. 53 for CO and from Ref. 54 for N_2. One can see the same trend for the calculated frequency-dependent quantities as in the case of static quantities. The LDA values are systematically too large (causing the LDA overestimations for

frequency-dependent properties to be even larger than for the static counterparts), the LB and LBα ones are too low, while SAOP provides the desired balance. The SAOP values are always the best, with the exception of the C_6 coefficient for CO, for which SAOP and LDA have nearly identical errors, and the Cauchy coefficients for C_2H_4, which are calculated with similar accuracy with SAOP and LBα SAOP produces an especially dramatic improvement for the frequency-dependent hyperpolarizabilities β and γ, for which earlier LDA and LB calculations gave unsatisfactory results.[21] In contrast, the present results are within, or very close to, the experimental error bounds in all cases.

It is important to note that the LBα and SAOP potentials not only improve the magnitude of the static hyperpolarizabilities, but also modify the relative frequency dependence with respect to the LDA and LB results. For example, in the case of C_2H_4 the SAOP frequency dependence of γ is larger than that of LB and smaller than that of LDA. This is what one would hope for on the basis of the known underestimation with LB of the frequency dependence of dipole polarizabilities. The fact that this characteristic is apparently improved by the SAOP potential is important, as there are only a few methods which provide correlated results for frequency-dependent hyperpolarizabilities and these are applicable to small molecules only. The frequency dependence of the dipole polarizability is also strongly improved in the case of CO and N_2, as can be seen from the Cauchy coefficients S_{-4} and S_{-6} (see Tables I and II). For those quantities, in particular, the SAOP error does not exceed 2%, ranging from 0.2% for S_{-6} of N_2 to 1.6% for S_{-6} of CO.

V. CONCLUSIONS

In this paper, the TDDFPT calculations of the polarizabilities and excitation energies for the prototype molecules CO, N_2, CH_2O, and C_2H_4 have been performed with the model Kohn–Sham exchange-correlation potential $\nu_{xc\sigma}^{SAOP}$ which is constructed with a statistical average of different model potentials $\nu_{xc\sigma}^{mod}$ for occupied KS orbitals (SAOP). The potentials $\nu_{xci\sigma}^{mod}$ are obtained with an interpolation between the modified LB potential $\nu_{xc\sigma}^{LB\alpha}$, which has the proper long-range Coulombic asymptotics, and the model potential $\nu_{xc\sigma}^{GLLB}$, which reproduces the atomic shell structure (in addition to being asymptotically correct). Thus, by construction, the model potential $\nu_{xc\sigma}^{SAOP}$ provides a balanced description of the electron exchange and correlation in both outer and inner atomic and molecular regions.

ν_{xc}^{SAOP} provides high quality results for a wide variety of response properties (linear and nonlinear response, static and frequency-dependent properties at both real and imaginary frequencies, both dipole and quadrupole polarizabilities) calculated for some prototype molecules. It gives a substantial improvement upon the LDA and LB potentials. In particular, the average error of the vertical excitation energies calculated with SAOP approaches the benchmark accuracy of 0.1 eV for the molecules CO, N_2, and CH_2O. Remarkably enough, the reported accuracy of the calculated frequency-dependent quantities is achieved solely by the improvement of the form of the XC potential ν_{xc}, while retaining the crude ALDA for the XC kernels f_{xc} and (in the case of the hyperpolarizabilities) g_{xc}. This confirms the conclusions of Ref. 11 concerning the relative importance of an accurate ν_{xc} as compared to f_{xc} and g_{xc}. The high quality results for the properties governing the frequency dependence, such as the Cauchy coefficients, are especially encouraging, as they show that the adiabatic approximation (the neglect of frequency dependence in the kernels f_{xc} and g_{xc}) is not a significant problem in these small molecules. Based on the present results, we propose to use the computationally efficient combination of the SAOP ν_{xc} with ALDA f_{xc} and g_{xc} in the calculations of molecular electronic spectra as well as for the investigation of various molecular NLO effects. The potential ν_{xc}^{SAOP} can also be used to study the time evolution of molecular systems within nonperturbative time-dependent KS theory (see Ref. 1 and references therein for examples).

The application of the SAOP potential to small molecules thus seems promising, but quite probably it will not solve the problems which are encountered in LDA/ALDA and GGA/ALDA calculations on long conjugated molecular chains. The LDA and GGA (hyper)polarizabilities on those systems are strongly overestimated, a problem which was first noted in Refs. 55,56 and analyzed it in detail in Ref. 27. In order to solve this problem, improvements to the xc kemels will be needed, perhaps in addition to improved xc potentials. It was noted in Ref. 27 that the KLI functional has a qualitatively different behavior from the LDA and GGA potentials and provides much better results. The improved behavior of the KLI functional is related to the atomic shell structure (''steps'') in its potential, which shows the importance of modeling this feature of the potential, as is done in the SAOP potential.

In future work, the transferability of these results to other systems and other molecular properties will be investigated. We trust that, if necessary, the flexibility of the SAOP approach will allow for a further fine-tuning, for example, in the inner core or far asymptotics regions. For instance, one can try to improve the performance of $\nu_{xc\sigma}^{SAOP}$ by further modifying its LBα part. Though $\nu_{xc}^{LB\alpha}$ has the proper Coulombic asymptotics, it might approach it in a suboptimal manner. Thus, a refinement of $\nu_{xc\sigma}^{SAOP}$ might be achieved by the replacement of $\nu_{xc}^{LB\alpha}$ at the far asymptotics with another potential ν_{xc}^{asymp}, which (like the Fermi–Amaldi potential employed in Ref. 5) approaches $-1/r$ in a different manner than ν_{xc}^{LB}. In the region of the near asymptotics $\nu_{xc}^{LB\alpha}$ can be retained and in the intermediate region a suitable interpolation between ν_{xc}^{asymp} and $\nu_{xc}^{LB\alpha}$ can be achieved with the dimensionless gradient x_σ employed as the interpolation parameter. Work along these lines is in progress.

[1] E. K. U. Gross, J. F. Dobson, and M. Petersilka, in *Density Functional Theory*, edited by R. F. Nalewajski (Springer-Verlag, Berlin, 1996), Vol. 181, p. 81.
[2] M. Casida, in *Recent Advances in Density Functional Methods*, edited by D. P. Chong (World Scientific, Singapore, 1995), Vol. 1.
[3] S. J. A. van Gisbergen, J. G. Snijders, and E. J. Baerends, J. Chem. Phys. **103**, 9347 (1995).
[4] R. Bauernschmitt and R. Ahlrichs, Chem. Phys. Lett. **256**, 454 (1996).
[5] D. J. Tozer and N. C. Handy, J. Chem. Phys. **109**, 10180 (1998).
[6] S. J. A. van Gisbergen, J. G. Snijders, and E. J. Baerends, Comput. Phys. Commun. **118**, 119 (1999).

[7] C. Jamorski, M. Casida, and D. R. Salahub, J. Chem. Phys. **104**, 5134 (1996).
[8] M. E. Casida, C. Jamorski, K. C. Casida, and D. R. Salahub, J. Chem. Phys. **108**, 4439 (1998).
[9] M. Petersilka, U. J. Gossmann, and E. K. U. Gross, Phys. Rev. Lett. **76**, 1212 (1996).
[10] R. Bauernschmitt, M. Haeser, O. Treutler, and R. Ahlrichs, Chem. Phys. Lett. **264**, 573 (1997).
[11] S. J. A. van Gisbergen, F. Kootstra, P. R. T. Schipper, O. V. Gritsenko, J. G. Snijders, and E. J. Baerends, Phys. Rev. A **57**, 2556 (1998).
[12] R. E. Stratmann, G. E. Scuseria, and M. J. Frisch, J. Chem. Phys. **109**, 8218 (1998).
[13] S. J. A. van Gisbergen, V. P. Osinga, O. V. Gritsenko, R. van Leeuwen, J. G. Snijders, and E. J. Baerends, J. Chem. Phys. **105**, 3142 (1996).
[14] V. P. Osinga, S. J. A. van Gisbergen, J. G. Snijders, and E. J. Baerends, J. Chem. Phys. **106**, 5091 (1997).
[15] U. Hohm, D. Goebel, and S. Grimme, Chem. Phys. Lett. **272**, 1059 (1997).
[16] A. Görling, H. H. Heinze, S. P. Ruzankin, M. Staufer, and N. Rösch, J. Chem. Phys. **110**, 2785 (1999).
[17] A. G. Ioannou, S. M. Colwell, and R. D. Amos, Chem. Phys. Lett. **278**, 278 (1997).
[18] S. J. A. van Gisbergen, J. G. Snijders, and E. J. Baerends, Phys. Rev. Lett. **78**, 3097 (1997).
[19] S. J. A. van Gisbergen, J. G. Snijders, and E. J. Baerends, J. Chem. Phys. **109**, 10644 (1998).
[20] S. J. A. van Gisbergen, J. G. Snijders, and E. J. Baerends, J. Chem. Phys. **111**, 6652 (1999).
[21] S. J. A. van Gisbergen, J. G. Snijders, and E. J. Baerends, J. Chem. Phys. **109**, 10657 (1998).
[22] A. J. Cohen, N. C. Handy, and D. J. Tozer, Chem. Phys. Lett. **303**, 391 (1999).
[23] K. B. Wiberg, R. E. Stratmann, and M. J. Frisch, Chem. Phys. Lett. **297**, 60 (1998).
[24] S. Hirata and M. Head-Gordon, Chem. Phys. Lett. **302**, 375 (1999).
[25] D. Sundholm, Chem. Phys. Lett. **302**, 480 (1999).
[26] R. Bauernschmitt, R. Ahlrichs, F. H. Hennrich, and M. K. Kappes, J. Am. Chem. Soc. **120**, 502 (1998).
[27] S. J. A. van Gisbergen, P. R. T. Schipper, O. V. Gritsenko, E. J. Baerends, J. G. Snijders, B. Champagne, and B. Kirtman, Phys. Rev. Lett. **83**, 694 (1999).
[28] A. Rosa, E. J. Baerends, S. J. A. van Gisbergen, E. van Lenthe, J. A. Groeneveld, and J. G. S. Snijders, J. Am. Chem. Soc. **121**, 10356 (1999).
[29] S. J. A. van Gisbergen, J. A. Groeneveld, A. Rosa, J. G. Snijders, and E. J. Baerends, J. Phys. Chem. A **103**, 6835 (1999).
[30] S. J. A. van Gisbergen, A. Rosa, G. Ricciardi, and E. J. Baerends, J. Chem. Phys. **111**, 2499 (1999).
[31] M. Petersilka, U. J. Gossmann, and E. K. U. Gross, in *Electronic Density Functional Theory: Recent Progress and New Directions*, edited by J. F. Dobson, G. Vignale, and M. P. Das (Plenum, New York, 1998), p. 177.
[32] I. Vasiliev, S. Ögüt, and J. R. Chelikowsky, Phys. Rev. Lett. **82**, 1919 (1999).
[33] S. A. C. McDowell, R. D. Amos, and N. C. Handy, Chem. Phys. Lett. **235**, 1 (1995).
[34] R. van Leeuwen and E. J. Baerends, Phys. Rev. A **49**, 2421 (1994).
[35] M. E. Casida, K. C. Casida, and D. R. Salahub, Int. J. Quantum Chem. **70**, 933 (1998).
[36] O. V. Gritsenko, P. R. T. Schipper, and E. J. Baerends, Chem. Phys. Lett. **302**, 199 (1999).
[37] O. V. Gritsenko, R. van Leeuwen, E. van Lenthe, and E. J. Baerends, Phys. Rev. A **51**, 1944 (1995).
[38] O. V. Gritsenko, R. van Leeuwen, and E. J. Baerends, Int. J. Quantum Chem. **61**, 231 (1997).
[39] A. Becke, Phys. Rev. A **38**, 3098 (1988).
[40] P. R. T. Schipper, O. V. Gritsenko, and E. J. Baerends, Theor. Chem. Acc. **98**, 16 (1997).
[41] J. P. Perdew, K. Burke, and Y. Wang, Phys. Rev. B **54**, 16533 (1996).
[42] J. P. Perdew, in *Electronic Structure of Solids*, edited by P. Ziesche and H. Eschrig (Akademie-Verlag, Berlin, 1991), p. 11.
[43] J. P. Perdew, J. A. Chevary, S. H. Vosko, K. A. Jackson, M. R. Pederson, D. J. Singh, and C. Fiolhais, Phys. Rev. B **46**, 6671 (1992).
[44] E. J. Baerends and O. V. Gritsenko, J. Phys. Chem. **101**, 5383 (1997).
[45] J. B. Krieger, Y. Li, and G. J. Iafrate, Phys. Rev. A **45**, 101 (1992).
[46] J. P. Perdew, R. G. Parr, M. Levy, and J. L. Balduz, Phys. Rev. Lett. **49**, 1691 (1982).
[47] R. van Leeuwen, O. V. Gritsenko, and E. J. Baerends, Top. Curr. Chem. **180**, 107 (1996).
[48] O. V. Gritsenko, P. R. T. Schipper, and E. J. Baerends, Int. J. Quantum Chem. (accepted).
[49] S. J. A. van Gisbergen, Ph.D. thesis, Vrije Universiteit, 1998.
[50] J. B. Foresman, M. Head-Gordon, J. A. Pople, and M. J. Frisch, J. Phys. Chem. **96**, 135 (1992).
[51] A. Savin, C. J. Umrigar, and X. Gonze, Chem. Phys. Lett. **288**, 391 (1998).
[52] C. Filippi, C. J. Umrigar, and X. Gonze, J. Chem. Phys. **107**, 9994 (1997).
[53] M. A. Spackman, J. Chem. Phys. **94**, 1288 (1991).
[54] G. D. Zeiss and W. J. Meath, Mol. Phys. **33**, 1155 (1977).
[55] B. Champagne, E. A. Perpete, S. J. A. van Gisbergen, E. J. Baerends, J. G. Snijders, C. Soubra-Ghaoui, K. A. Robins, and B. Kirtman, J. Chem. Phys. **109**, 10489 (1998).
[56] B. Champagne, E. A. Perpete, S. J. A. van Gisbergen, E. J. Baerends, J. G. Snijders, C. Soubra-Ghaoui, K. A. Robins, and B. Kirtman, J. Chem. Phys. **110**, 11664 (1999).